





Cite this: *Nanoscale*, 2018, **10**, 20453

## Specific binding and internalization: an investigation of fluorescent aptamer-gold nanoclusters and cells with fluorescence lifetime imaging microscopy†

Marina Mutas,<sup>a,b</sup> Christian Strelow,<sup>a</sup> Tobias Kipp \*<sup>a</sup> and Alf Mews <sup>a</sup>

Fluorescent gold nanoclusters show promising properties for biological applications. We biofunctionalized fluorescent 11-mercaptopundecanoic-acid stabilized gold nanoclusters (AuNCs) with an aptamer to target the interleukin-6-receptor expressed on BaF3 cells specifically. Although the fluorescence emission of the AuNCs (535 nm) is in the same wavelength region as the autofluorescence of the cell, we are able to distinguish between nanoclusters and cells using the fluorescence decay time, which is much longer for the AuNCs (100 ns) than for the autofluorescence. After a first short incubation period we detected AuNCs specifically bound to the cell membrane by using two fluorescence lifetime imaging microscopy (FLIM) methods: gated and direct FLIM. After a second incubation period the previously bound AuNCs are internalized by the cells, as could be resolved solely by the direct FLIM. This proves the superior sensitivity of this method compared to gated FLIM. We find that the optical properties of AuNCs do not change upon binding to the cells, but exhibit a change when internalized into the cells, induced by an interaction between the AuNCs and cells.

Received 16th August 2018,  
Accepted 6th October 2018

DOI: 10.1039/c8nr06639f

rscl.li/nanoscale

### 1. Introduction

Fluorescent nanoclusters are promising novel fluorescent materials for biological applications. In particular, gold nanoclusters (AuNCs) combine promising chemical and physical properties like simple preparation, high photostability, good biocompatibility, and size-dependent emission wavelength making them useful in a variety of biomedical applications including sensing, diagnostics, and cell imaging.<sup>1–6</sup> Size tunability is achieved only for very small Au<sub>5</sub> to Au<sub>55</sub> clusters.<sup>7,8</sup> The specific choice of stabilizing ligands for AuNCs offers a further degree of freedom to tune the emission wavelength, which is also available for larger AuNCs.<sup>9,10</sup> Furthermore, the ligands allow for a high degree of flexibility in terms of functional groups for biofunctionalization and targeting. Due to their strong affinity to noble metals, thiol molecules are commonly used as ligands for synthesizing, stabilizing, and functionalizing AuNCs.<sup>11,12</sup>

Thiol-containing peptides, organosulfur compounds, polymers, and amino acids have already been used as stabilizing ligands for fluorescent AuNCs.<sup>13</sup> These ligands additionally offer flexible functional groups for biofunctionalization and targeting for specific biomedical purposes.<sup>1,5,14–16</sup>

Glutathione stabilized fluorescent AuNCs, for example, show a high specificity to MCF7 breast cancer cells. Loaded with doxorubicin, an anti-cancer drug, the glutathione-AuNCs functioned as a therapeutic nanomaterial and only selectively killed the cancer cells.<sup>17</sup> It has also been reported that small (1–2 nm in diameter) zwitterionic AuNCs show a high uptake rate with a combined low cytotoxicity in dendritic cells.<sup>18</sup> Several other publications also demonstrate the possible application of fluorescent thiol-stabilized AuNCs for cancer-cell targeting and imaging.<sup>1,5,14,15</sup> However, in all cases a high AuNC concentration (in a  $\mu\text{M}$  range) and a long incubation period ( $\geq 1$  hour) were applied, making use of the general properties of cells to take up various types of nano-objects unspecifically.

For biomedical applications, high specificities are necessary to allow for an efficient targeted drug delivery. Specificity can be achieved by biofunctionalization of AuNCs with molecular targeting ligands that can bind to their target sites on the cancer cell membrane. Kong *et al.*, for example, were able to image near-infrared emitting vitamin B<sub>12</sub>-R-AuNCs that were specifically internalized into Caco-2 cells by receptor-mediated endocytosis.<sup>19</sup> Li and coworkers used a computer tomography

<sup>a</sup>Institute of Physical Chemistry, University of Hamburg, Grindelallee 117, Hamburg, Germany. E-mail: kipp@chemie.uni-hamburg.de; Tel: +49 40 42838 8277

<sup>b</sup>The Hamburg Centre for Ultrafast Imaging, Luruper Chaussee 149, 22761 Hamburg, Germany

†Electronic supplementary information (ESI) available. See DOI: 10.1039/C8NR06639F







attack the NHS ester is then easily displaced and a stable amide bond is formed.

The green curve in Fig. 1(a) shows the UV-Vis absorption spectrum after the cross-linking of the AIR-3A aptamer to the MUA ligand. The absorption shoulder at a wavelength of 270 nm of the Sulfo-NHS ester vanished and the characteristic absorption maximum for RNA sequences appeared at 260 nm.<sup>34</sup> The difference in the wavelength of the absorption feature of the Sulfo-NHS ester (shoulder in spectrum 2) and of the aptamer (peak in spectrum 3) is small but sufficient to prove the successful biofunctionalization. The biofunctionalized AIR-3A-MUA-AuNCs are called aptamer-AuNCs in the following.

Fig. 1(c) shows the fluorescence spectra of aptamer-AuNCs (green curve) and the autofluorescence of a BaF3 cell (black curve). The aptamer-AuNCs display a fluorescence peaking at a wavelength of 535 nm, which is similar to unfunctionalized 11-MUA-AuNCs (see Fig. S1(b)†). The fluorescence emission strongly overlaps with the autofluorescence spectrum of BaF3 cells making it difficult to distinguish between emission from the aptamer-AuNCs and the cells.

Fig. 1(d) displays the fluorescence decay curves of the aptamer-AuNCs (green) and a BaF3 cell (black). The fluorescence decay of aptamer-AuNCs exhibits an average lifetime of around 110 ns while the autofluorescence only shows

average lifetimes between 2 and 3 ns. This significant difference in lifetime enables us to distinguish between the autofluorescence of the cell and the emission of the AuNCs by FLIM. In contrast to common fluorescence microscopy, where different fluorophores are distinguished by their emission wavelengths, FLIM produces images encoding different arrival times of photons after pulsed laser excitation.<sup>35,36</sup>

### 3.2. Selective attachment during the first incubation

For a specific interaction we incubated BaF3 cells with aptamer-AuNCs at 37 °C for 10 min. Dark field and scanning electron microscopy images as well as the atomic force microscopy cross section of a BaF3 cell are given in ESI Fig. S2.† Also, we verified the biocompatibility of the 11-MUA-AuNCs by a simple cell viability assay (see ESI, Fig. S1(c)†). The preparation procedure is shown in Fig. 2(a), more details are given in the Materials and methods section. In a previous work, we found that an incubation time of 10 min showed the highest specificity for 7 nm-sized aptamer-biofunctionalized, non-fluorescent gold nanoparticles for the IL-6R expressed on the BaF3 cells.<sup>37</sup> The investigation by ICP-MS did not allow for the localization of the nanoparticles.

Fig. 2(c) and (d) show the FLIM images of a BaF3 cell incubated with aptamer-AuNCs after washing and fixation.



**Fig. 2** Sketches of (a) the incubation process of BaF3 cells with aptamer-AuNCs and (b) the three measured axial ( $z$ ) levels within the cell. BaF3 cells were incubated for 10 min at 37 °C with aptamer-AuNCs, then washed three times to remove any excess of AuNCs, and fixed. (c) Gated and (d) direct FLIM images of a BaF3 cell with aptamer-AuNCs at axial levels  $z = 0.0, 1.0,$  and  $3.0 \mu\text{m}$ . (e) Fluorescence decay curves corresponding to the areas encircled in (d) (1–3; orange, red, blue) fitted by decay curves (grey) calculated by superimposing the autofluorescence curve (black) and fluorescence curve of aptamer-AuNCs (green) with adjusted weighting ratios. Scale bars are  $2 \mu\text{m}$ .





single AuNCs we investigated individualized AuNCs. Combining confocal fluorescence measurements with atomic force microscopy and element specific scanning electron microscopy we could estimate that the detection limit lies above a few hundreds of AuNCs in one patch (see ESI Fig. S7†). Although we were not able to quantify the intensity of individual AuNCs, this proves that the sharp features arise from many AuNCs. This conclusion is also supported by ICP-MS measurements. We determined the amount of gold to be  $1.04 \times 10^6$  AuNCs per cell, assuming a AuNC diameter of 1.9 nm. To illustrate the meaning of this number, we also calculated the fraction of the cell surface that would be covered with AuNCs if all these AuNCs would be arranged in a monolayer on top of the cell surface. We found this value to be 7.3% assuming a cell with a diameter of 10  $\mu\text{m}$ , which is a reasonable result with respect to the FLIM images in Fig. 2(c) and (d).

Regarding (ii), our results strongly imply a specific binding of aptamer-AuNCs to the surface of BaF3 cells after the first incubation step: the sharp features that are dominant in gated FLIM images with a long timeframe and appear green in direct FLIM images are always located around the region of strong autofluorescence, the latter visible only in gated FLIM images with a short timeframe and colored red in the direct FLIM. If the patches of AuNCs were located inside the cell, they should become visible for intermediate z-positions and disappear for

higher z-positions. At the same time autofluorescence of the cell should be present at lower and higher z-positions than the position of AuNCs. We would also expect that the color in the direct FLIM images of AuNCs inside a cell should be different from AuNCs on the cell membrane since the emission of the AuNCs inside the cell is mixed with a higher amount of autofluorescence.

With gated and direct FLIM we are able to visualize the specific binding of biofunctionalized AuNCs to the IL-6R expressed on BaF3 cells after only 10 min at 37 °C. Since no internalized AuNCs could be observed in gated and direct FLIM images, we introduced a second incubation step and investigated further.

### 3.3. Internalization after a second incubation

In order to address internalization of AuNCs in more detail we expanded the above-described experiment by a further incubation step. Fig. 3(a) schematically shows the preparation procedure. Principally, the first steps of the preparation were the same as for the single incubated samples: after incubation and washing, which removes unbound aptamer-AuNCs, the majority of the AuNCs is attached to the cell membrane and (nearly) no AuNCs are internalized into the cell. In the next step we incubated again for 10 min at 37 °C, but without adding aptamer-AuNCs. The idea behind this is that the pre-

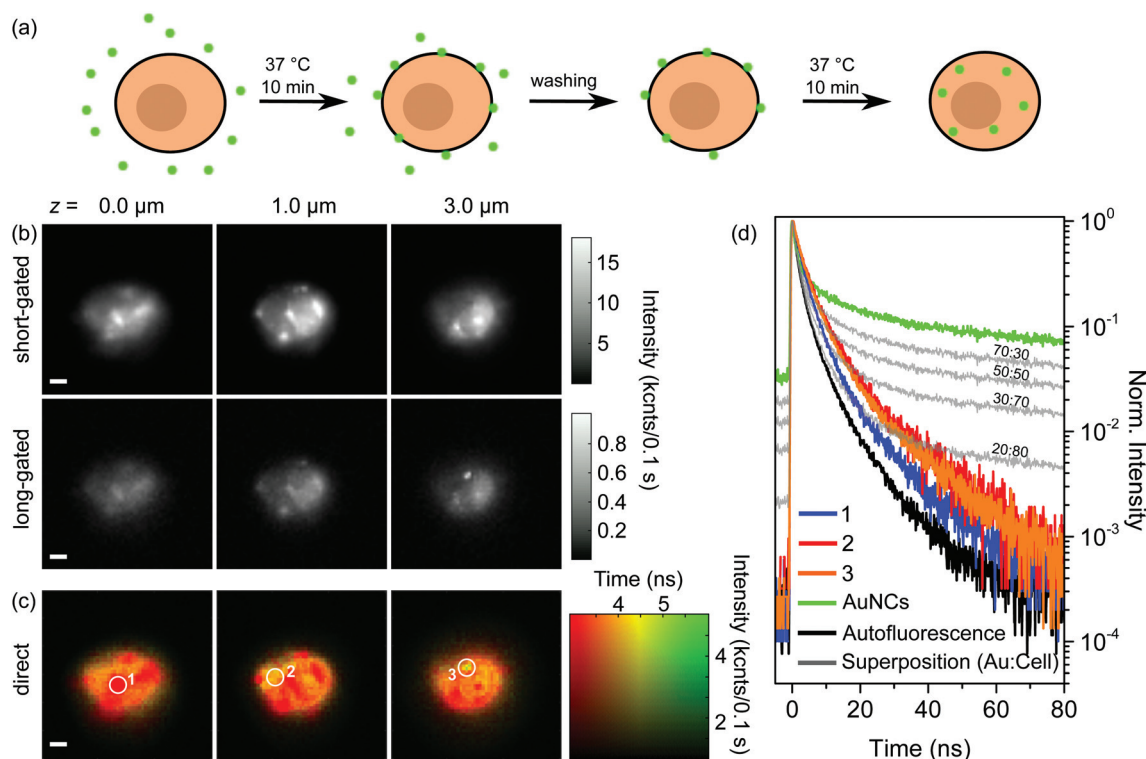


**Fig. 3** (a) Sketches of the incubation process of BaF3 cells with aptamer-AuNCs. BaF3 cells were incubated for 10 min at 37 °C in a 4.7 nM aptamer-AuNC solution, washed three times to remove any excess of AuNCs, and then again incubated for 10 min at 37 °C without any addition of aptamer-AuNCs. (b) Gated and (c) direct FLIM images of two times incubated BaF3 cell aptamer-AuNCs at axial  $z = 0.0, 1.0,$  and  $3.0 \mu\text{m}$ . (d) Fluorescence decay curves corresponding to the encircled areas in (c) (1–3, orange, red, blue) compared to decay curves (grey) calculated by superimposing the autofluorescence curve (black) and fluorescence curve of aptamer-AuNCs (green) with adjusted weighting ratios. Scale bar 2  $\mu\text{m}$ .



viously attached aptamer-AuNCs might get internalized as shown in Fig. 3(a).

In Fig. 3(b) and (c) we show the results of gated and direct FLIM measurements of a BaF3 cell after the second incubation step. The three heights above the substrate, the particular timeframes for gated FLIM images, and the time and intensity scaling for direct FLIM images were chosen to be the same as for Fig. 2(c) and (d). The FLIM images of all measured heights (10 levels between 0.0 and 4.5  $\mu\text{m}$ ) are shown in the ESI in Fig. S8.†

In the FLIM images with short timeframes in Fig. 3(b) we find again the blurred circular-shaped pattern typical of the autofluorescence signal of the cell. Additionally, a few sharp features of AuNCs are visible, similar to the situation in Fig. 2(c). In contrast, some of the features also appear in the center part of the cell (*cf.* Fig. 2(c) and 3 (b) at  $z = 1.0 \mu\text{m}$ ). In gated FLIM images with a long gate the sharp features do not become as prominent as in the corresponding Fig. 2(c). Moreover, the overall intensity is strongly reduced. Note that the intensity range is scaled down by a factor of more than 15 compared to the image with a short timeframe. Only for a height of 3.0  $\mu\text{m}$ , which corresponds to the top of the cell, a sharp feature becomes apparent. In the gated FLIM images, we observe no attached aptamer-AuNCs except for the one spot on top of the cell. Also, we cannot identify any internalized AuNCs. Consequently, from the gated FLIM images in Fig. 3(b) we are not able to make a statement concerning the localization of the AuNCs.

An explanation for not being able to localize the AuNCs could be the detachment of AuNCs from the IL-6R during the second incubation step. As a control experiment we performed ICP-MS measurements, similar to already described above. Instead of  $1.04 \times 10^6$  AuNCs per cell that we received for the single incubation, we obtained a value of  $0.73 \times 10^6$  AuNCs per cell. This means that instead of 16% of the total amount of gold, we still measure 11% after the second incubation step. The ICP-MS investigation shows that the vast majority of aptamer-AuNCs are still on or in the cells. An extensive detachment of AuNCs as being the reason for the absence of the sharp features in long-gated FLIM images can be excluded. The slightly decreased amount of the AuNCs after the second incubation step can easily be explained by the additional washing step and exocytosis. Hence, aptamer-AuNCs are still on and in the cells. Another scenario that could explain the absence of the sharp features could be that aptamer-AuNCs are still bound to the cell membrane while they lost their fluorescence properties due to chemical degradation during the second incubation step. We reviewed this possibility with control experiments: exposing aptamer-AuNCs for 20 min at 37 °C just in buffer or with cells in a single incubation step still showed fluorescence behaviour. Furthermore, since the treatment of aptamer-AuNCs and cells during the second incubation step is the same as during the first incubation step we can exclude a chemical degradation during the second incubation step.

Summarizing the results for the gated FLIM images, we can only indirectly conclude that a considerable part of the previously attached aptamer-AuNCs has been internalized during the second incubation step, but a direct proof is missing. Fig. 3(c) shows the direct FLIM images. The first and most important observation is that in the direct FLIM representation, instead of predominant sharp green features found after the first incubation step, most of the cells are now colored orange, indicating lifetimes of around 4.5 ns. Furthermore, the orange-colored regions are found for all heights. Only a few parts of the cell show a red color indicating dominant autofluorescence with a lifetime of about 3 ns or less. Interestingly, these regions coincide with sharp features visible in the gated FLIM images, in clear contrast to the images after the first incubation step, where sharp features were colored green. Only a single small green spot is visible for a height of 3.0  $\mu\text{m}$  (white circle), coinciding with the sharp feature prominent in the FLIM image with a long timeframe at  $z = 3.0 \mu\text{m}$ .

The first fundamental conclusion from observing an orange color in direct FLIM images is that aptamer-AuNCs are still emitting fluorescence. Furthermore, since we observe orange color for all heights, we conclude that aptamer-AuNCs have to be inside the cell. This is direct proof of successful internalization of aptamer-AuNCs into the BaF3 cells, which is not visible in the gated FLIM images. The orange color appears in rather large regions of the cell. This shows that the AuNCs are not strongly localized in only a few regions inside the cell. Based on our results we propose the following course of events: during the first incubation step, islands of aptamer-AuNCs are specifically bound to the surface of the cells (visible as green spots in direct FLIM images) while nearly no or only a few AuNCs are internalized into the cell. During the second incubation step, the previously bound patches are internalized into the cell. We expect the AuNCs to be internalized by receptor-mediated endocytosis.<sup>32,33,38</sup> One might speculate that the AuNCs are located in many endosomes as well as lysosomes with their spatial distribution being connected to the orange-colored regions observed in the direct FLIM images. Instead of internalization, a few of the bound AuNCs could also have detached from the IL-6R and eventually bound again to another receptor (which could explain the small green spot on top of the cell in Fig. 3(c)).

Summarizing the different FLIM methods, we find that gated FLIM was not capable of giving direct proof of the internalization of AuNCs into the cell, while the direct FLIM method is. It is worth mentioning again that both FLIM methods rely on the very same data set that is differently expressed.

### 3.4. Cell–AuNC interaction

We now want to analyze the lifetime data for selected points of FLIM images in more detail to gain further insight into the optical properties of AuNCs either attached to or internalized into the cells. Fig. 2(e) shows the decay curves of the selected positions marked by white circles in the direct FLIM images in







